A Nonlinear Dynamic Model With Confidence Bounds for Hydrodynamic Bearings

Chin S. Chu
Graduate Research Assistant.

Kristin L. Wood
Associate Professor.

Ilene J. Busch-Vishniac
Professor.

Department of Mechanical Engineering,
The University of Texas,
Austin, TX

In conventional rotordynamic modeling, hydrodynamic bearings are often characterized by a set of linear stiffness and damping coefficients obtained from a first-order Taylor series expansion of bearing reactions. Theoretically, these coefficients are only valid for small amplitude motion about an equilibrium position. In this paper, a nonlinear dynamic model that overcomes the small amplitude assumption in the conventional linear analysis is described. By including higher-order terms in the bearing reaction expansion, nonlinearity in the oil film forces for large amplitude motion can be captured and represented by a set of nonlinear stiffness and damping coefficients. These coefficients are functions of static bearing displacement. A finite difference approach is described and is used to solve for these coefficients. The stated model is applied to a conventional slider bearing and a mechanical smart slider bearing that experiences large variations in load. Error assessment is performed numerically on the higher-order solutions to determine an acceptable displacement bound for the higher order coefficients.

1 Introduction

There are generally two approaches to representing fluid film bearings in rotordynamic modeling: namely, a linearized model and a time-transient model (Shapiro and Rumbarger, 1971). The linearized model represents bearing systems by constant stiffness and damping coefficients evaluated about a nominal operating position. Dynamic response and stability conditions can be evaluated using a time-invariant linear dynamic model with these stiffness and damping coefficients. The time-transient model, on the other hand, produces a time history of the bearing displacement in all degrees of freedom without any linearization assumptions. The latter approach provides the closest simulation of the actual system performance; however, repetitive solution of the governing fluid equation is required over a time span, resulting in costly computational requirements. It is therefore a common practice to use the linearized approach unless the linearized assumption deteriorates, i.e., when the bearing motion amplitude becomes large.

In some cases, the linearized model may be shown to be valid over a range of bearing parameters and operating conditions. Shapiro and Rumbarger (1971) suggest that displacements over 10 percent of the operating film thickness would require appropriate modification of linear spring and damping constants. Lund (1987), who introduced the linearized bearing analysis, states that the linear coefficients maybe valid for amplitudes up to 40 percent of bearing minimum clearance. However, there is no justification of his criterion in terms of coefficient accuracy at such high displacement amplitudes. Obviously, such a linearized approach would require an evaluation of the linearized error to set forth an acceptable bound for the linear solutions. Hashi and Sankar (1984) have attempted to estimate the linearized error. Deviations of linearized journal bearing coefficients from the nonlinear systems are calculated. Error estimation charts for some important cases of plain journal bearings under unbalance loading are provided.

When the bearing displacement amplitude exceeds a certain limit, bearing reactions become nonlinear. There are limited studies which have been performed on the nonlinearity within the bearing oil film. Hattori (1993) shows that for a rotary compressor under large dynamic loads (displacement amplitude varies more than 50 percent of the radial clearance per revolution), journal bearing stiffness and damping coefficients can vary by more than one order of magnitude, demonstrating that oil film nonlinearity seriously influences rotor motion. The linearized model is therefore not acceptable for such cases and some form of nonlinear analysis is required. Choy, et al. (1991) use a nonlinear approach in modeling the nonlinearity within the oil film forces. They expand the bearing reactions using a power series and retain the higher order terms. They show that at displacements far away from the equilibrium, nonlinearity in the oil film is significant and can be modeled closely by higher order stiffness and damping coefficients. Their results indicate that the range of accuracy for the higher-order coefficients can be extended by including more terms in the expansion.

In this paper, a quasi-static nonlinear dynamic model for hydrodynamic bearings is described. There are two features to this model: (*i*) a nonlinear dynamic model capable of capturing the nonlinearity in oil film forces under large amplitude excursions, and (*ii*) an error scheme that evaluates higher-order truncation error in the oil film force expansion. The first feature enables the designer to calculate the nonlinear oil film forces. The second feature provides a useful way for the designer to set a confidence bound on the nonlinear solutions. Depending on the application requirements, additional terms can be added to the bearing load expansion.

A finite difference scheme with successive-over-relaxation (SOR) is employed to solve the stated nonlinear model. This model is first applied to a conventional slider bearing to benchmark the new model and then to a new Micro-Electro-Mechanical Systems (MEMs) smart bearing concept (Hearn et al., 1995). The MEMs smart bearing concept involves active control of the film thickness profile to induce desirable bearing performance. A typical MEMs smart bearing consists of an actively deformable surface (actuators) and pressure sensors (Hearn et al., 1995). Preliminary results from a linear model

Contributed by the Tribology Division for publication in the JOURNAL OF TRIBOLOGY. Manuscript received by the Tribology Division June 7, 1995; revised manuscript received June 16, 1997. Associate Technical Editor: M. J. Braun.

indicate that MEMs smart bearing's minimum clearance could vary as much as 30 percent upon the actuation of the deformable surface. The nonlinear model described in this paper is well suited for this bearing because of the large amplitude excursion experienced by the bearing during the actuation process. Other potential applications of the present modeling approach include modeling of dynamic loading on a journal bearing within a rotary compressor (Hattori, 1993) or other smart bearing concepts such as the one developed by Rylander, et al. (1995). In the latter example, a smart bearing concept that can reduce bearing vibration amplitudes through an active transformation of journal bearing form is tested. This bearing experiences large amplitude excursions that can be modeled by the present approach.

2 Analysis

In this section, the modeling approach is first discussed, and the formulation of a 1-D quasi-static nonlinear dynamic model is detailed. The remaining sections present a description of the numerical solution scheme, the solution procedure, and the specific application of the 1-D nonlinear dynamic model in a MEMs smart bearing.

2.1 Modeling Concept. Most of the analysis of the dynamic characteristics of hydrodynamic bearings involves linearization of oil film forces about an static equilibrium position using a first-order Taylor series expansion (Lund, 1987; Hamrock, 1994). This approach assumes that the dynamic amplitude of the rotor center motion is negligible. However, when the rotor center is experiencing large variations in dynamic load, the rotor motion amplitudes cannot be ignored. Then, linear coefficients obtained at one position are meaningless. In this case, if the higher-order terms in the Taylor series expansion are retained, the bearing load becomes a nonlinear function of rotor displacement and rotor velocity up to any desirable order. Such a model is valid even for large dynamic motion amplitudes. Depending on the designer's application ranges, the order of the expansion can be adjusted accordingly through a truncation error evaluation. In terms of system representation, the bearing system can be conveniently represented by a set of nonlinear stiffness and nonlinear damping coefficients defined from the classical definitions of stiffness and damping coefficients. This allows the representation of bearing dynamic characteristics without regard to a particular rotor system. Such a representation depends on bearing geometry as presented in the next section.

2.2 Geometry, Fluid Model, and Equation of Motion. A slider bearing model is used to demonstrate the development of a nonlinear dynamic model. The present approach is general and applies equally well for a journal bearing geometry. Figure 1 depicts a conventional smooth slider bearing. The bearing pad is rectangular in shape with length L and breadth B. The bearing is characterized by an inlet-to-outlet ratio (h_i/h_o) and has a runner velocity U. The two dimensional dynamic pressure distribution within the bearing gap $P(x, y, t)$ is governed by the time dependent Reynolds' equation (Hamrock, 1994; Pinkus and Sternlicht, 1961):

$$\frac{\partial}{\partial x}\left[h^3\frac{\partial P}{\partial x}\right]+\frac{\partial}{\partial x}\left[h^3\frac{\partial P}{\partial x}\right]=6\mu U\frac{\partial h}{\partial x}+12\mu\frac{\partial h}{\partial t}, \quad (1)$$

Nomenclature

h_i = inlet film thickness
h_0 = outlet or minimum film thickness
h = film thickness at each location
P = time dependent fluid film pressure
W = time dependent bearing load
t = time
L = bearing pad length
B = bearing pad breadth
μ = lubricant viscosity
U = bearing runner speed
m = mass of the bearing system
$b_{\dot{z}}$ = linear damping
k_z = linear stiffness
$f(t)$ = forcing function
z = displacement
$\dot{z}$ = velocity
Δz = perturbed displacement
$\Delta\dot{z}$ = perturbed velocity
z_o = arbitrary displacement operating point
$\dot{z}_o$ = arbitrary velocity operating point
W_o = steady state load
$k_z, k_{zz}, \ldots$ = stiffness terms
$b_{\dot{z}}, b_{z\dot{z}}, \ldots$ = damping terms
$c_{z\dot{z}}, c_{zz\dot{z}}, \ldots$ = cross-coupling terms
h_s = initial steady state film thickness
$P_o, P_z, P_{\dot{z}}, \ldots$ = perturbed pressures
L, L_o, L_1, L_2 = operator for expansion relations
I = integral operator ($I[\,] = \int_0^B \int_0^L [\,]dxdy$.)
k_{nl} = nonlinear stiffness
b_{nl} = nonlinear damping
E = perturbation error function
E_{norm} = normalized error within a perturbation space
$\bar{h} = h/h_o$ = normalized film thickness
$\bar{x} = x/L$ = normalized length coordinate
$\bar{y} = y/B$ = normalized breadth coordinate
f_n = source terms for the standard Reynolds' equation
$\bar{P}_n$ = normalized perturbed pressures
$\bar{W}_o$ = normalized steady state load
$\bar{k}_z, \bar{k}_{zz}, \ldots$ = normalized stiffness terms
$\bar{b}_{\dot{z}}$ = normalized linear damping
$\bar{c}_{z\dot{z}}, \bar{c}_{zz\dot{z}}, \ldots$ = normalized cross-coupling terms
$a_{i,j}, \ldots, f_{i,j}$ = coefficients for the finite difference formulation
$\bar{E}$ = normalized error function
$\bar{P}$ = normalized pressure
$\Delta\bar{z} = \Delta z/ho$ = normalized displacement
$\Delta\bar{\dot{z}} = \Delta\dot{z}/U \times (L/h_o)$ = normalized velocity
P_o = static pressure
ΔP = dynamic pressure
(x^*, y^*) = caviation boundary
ω_{SOR} = over-relaxation factor
$r_{i,j}$ = residual error at i, j
ρ_{Jacobi} = spectral radius of a Jacobi iteration
$\Delta\bar{x}, \Delta\bar{y}$ = step sizes in the $\bar{x}$ and $\bar{y}$ directions
i_{max}, j_{max} = number of grid points in the i and j directions
h_m = central film thickness for a tapered land thrust bearing
φ = sector pad inclination angle
r_o = sector pad outer radius
r_i = sector pad inner radius
α = sector angle
$\bar{W}_s$ = normalized nonlinear steady load
$\bar{k}_{nl}$ = normalized nonlinear stiffness
$\bar{b}_{nl}$ = normalized nonlinear damping
w = membrane feature actuation height

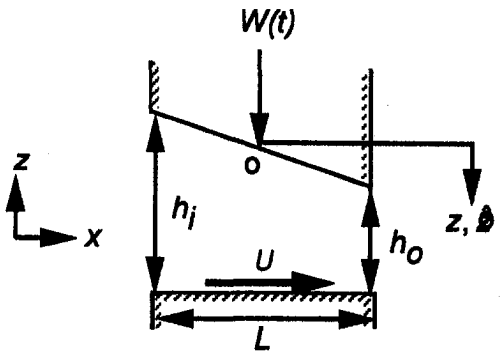

Fig. 1 Conventional slider bearing

where

$$h(x, y) = h_i - (h_i - h_o)\frac{x}{L} \tag{2}$$

is the oil film thickness at each location and the bearing reaction load W is obtained through

$$W(x, y, t) = \int_0^B \int_0^L P(x, y, t)\, dxdy. \tag{3}$$

This model is valid for isoviscous incompressible fluids. It is time dependent and can only be solved with the knowledge of the system equation of motion (time-transient approach).

For a slider bearing with one-dimensional (1-D) loading, the equation of motion given by Newton's second law is simply

$$m\ddot{z} + b_{\dot{z}}\dot{z} + k_z z = f(t), \tag{4}$$

where m is mass of the system, $b_{\dot{z}}$ is bearing damping, k_z is bearing stiffness, and $f(t)$ is bearing forcing, respectively.

2.3 1-D Quasi-Static Nonlinear Dynamic Model. To avoid the time-dependency of the above model (Eqs. (1)–(4)), a quasi-static approach is used to condense the time scale. In 1-D loading, it appears that bearing reaction is a function of the system states: displacement z and velocity $\dot{z}$. Applying standard perturbation theory, when the bearing vibrates with excursions Δz and $\Delta\dot{z}$, the bearing reaction can be expanded using a Taylor series expansion up to order n,

$$W(z_o + \Delta z, \dot{z}_o + \Delta\dot{z}) = W_o + \frac{\partial W}{\partial z}(\Delta z) + \frac{\partial W}{\partial \dot{z}}(\Delta\dot{z}) + \frac{1}{2}\frac{\partial^2 W}{\partial^2 z}(\Delta z)^2 + \frac{1}{2}\frac{\partial^2 W}{\partial^2 \dot{z}}(\Delta\dot{z})^2 + \frac{\partial^2 W}{\partial z \partial \dot{z}}(\Delta z)(\Delta\dot{z}) + O[(\Delta z)^3, (\Delta\dot{z})^3] \tag{5}$$

or

$$W(z_o + \Delta z, \dot{z}_o + \Delta\dot{z}) = W_o + k_z(\Delta z) + b_{\dot{z}}(\Delta\dot{z}) + \tfrac{1}{2}k_{zz}(\Delta z)^2 + \tfrac{1}{2}b_{\dot{z}\dot{z}}(\Delta\dot{z})^2 + c_{z\dot{z}}(\Delta z)(\Delta\dot{z}) + O[(\Delta z)^3, (\Delta\dot{z})^3], \tag{6}$$

where k denotes stiffness terms dependent solely on Δz, b denotes damping terms dependent solely on $\Delta\dot{z}$, and c denotes cross-coupling terms. The indices indicate the origin and the order of the terms. In Eq. (6), the first two linear terms are the familiar linear stiffness and linear damping. In contrast to the conventional linearized theory, this treatment maintains the expansion terms above first order in the system to capture the nonlinearity within the oil film forces.

The rotor excursions give rise to a perturbation in the film thickness. The new film thickness can be expressed as

$$h = h_s + \Delta z, \tag{7}$$

where h_s denotes the initial steady state film thickness. Since Δz is not a function of x, and the initial steady state film thickness is not a function of t, the following is true:

$$\frac{\partial h}{\partial x} = \frac{\partial h_s}{\partial x}; \tag{8}$$

$$\frac{\partial h}{\partial t} = \frac{\partial(\Delta z)}{\partial t} = \Delta\frac{\partial z}{\partial t} = \Delta\dot{z}. \tag{9}$$

Likewise, the perturbation in the film thickness gives rise to a similar perturbation in the oil film pressure P. Again, the pressure can be expressed by Taylor series expansion as

$$P(z_o + \Delta z, \dot{z}_o + \Delta\dot{z}) = P_o + \frac{\partial P}{\partial z}(\Delta z) + \frac{\partial P}{\partial \dot{z}}(\Delta\dot{z}) + \frac{1}{2}\frac{\partial^2 P}{\partial^2 z}(\Delta z)^2 + \frac{1}{2}\frac{\partial^2 P}{\partial^2 \dot{z}}(\Delta\dot{z})^2 + \frac{\partial^2 P}{\partial z \partial \dot{z}}(\Delta z)(\Delta\dot{z}) + O[(\Delta z)^3, (\Delta\dot{z})^3],$$

or

$$P(z_o + \Delta z, \dot{z}_o + \Delta\dot{z}) = P_o + P_z(\Delta z) + P_{\dot{z}}(\Delta\dot{z}) + \tfrac{1}{2}P_{zz}(\Delta z)^2 + \tfrac{1}{2}P_{\dot{z}\dot{z}}(\Delta\dot{z})^2 + P_{z\dot{z}}(\Delta z)(\Delta\dot{z}) + O[(\Delta z)^3, (\Delta\dot{z})^3]. \tag{10}$$

Substituting Eqs. (7)–(9) and 11 into the time-dependent Reynolds' equation (Eq. (1)), and expanding and collecting like order terms, we obtain a set of relationships for the calculation of higher-order perturbed pressures. Introducing the following operator notation,

$$L[\,] = \frac{\partial}{\partial x}\left[(h_s)^3\frac{\partial[\,]}{\partial x}\right] + \frac{\partial}{\partial y}\left[(h_s)^3\frac{\partial[\,]}{\partial y}\right],$$

$$L_0[\,] = \frac{\partial}{\partial x}\left[\frac{\partial[\,]}{\partial x}\right] + \frac{\partial}{\partial y}\left[\frac{\partial[\,]}{\partial y}\right],$$

$$L_1[\,] = \frac{\partial}{\partial x}\left[3h_s\frac{\partial[\,]}{\partial x}\right] + \frac{\partial}{\partial y}\left[3h_s\frac{\partial[\,]}{\partial y}\right],$$

$$L_2[\,] = \frac{\partial}{\partial x}\left[3(h_s)^2\frac{\partial[\,]}{\partial x}\right] + \frac{\partial}{\partial y}\left[3(h_s)^2\frac{\partial[\,]}{\partial y}\right], \tag{11}$$

these relationships through second order ($n = 2$) are

$$\begin{aligned}
&O[1] && L[P_o] = 6\mu U\frac{\partial h_s}{\partial x},\\
&O[\Delta z] && L[P_z] = -L_2[P_o],\\
&O[\Delta\dot{z}] && L[P_{\dot{z}}] = 12\mu,\\
&O[(\Delta z)^2] && L[\tfrac{1}{2}P_{zz}] = -L_2[P_z] - L_1[P_o],\\
&O[(\Delta\dot{z})^2] && L[\tfrac{1}{2}P_{\dot{z}\dot{z}}] = 0,\\
&O[\Delta z, \Delta\dot{z}] && L[P_{z\dot{z}}] = L_2[P_{\dot{z}}].
\end{aligned} \tag{12}$$

The first relationship, $O(1)$, is the familiar steady-state Reynolds' equation without the time-dependent term. The displacement related terms are functions of the wedge term ($\partial h_o/\partial x$) (Someya, 1989). On the other hand, the velocity and cross-coupling terms are functions of the squeeze term ($\partial h_o/\partial t$) (Someya, 1989). In terms of computation, not every relationship

in (12) needs to be solved. Those relationships with source terms equal to zero will have a trivial solution of zero value, for instances, $P_{\dot{z}\ddot{z}} = 0$.

Once the pressure derivatives are known, the nonlinear pressure expansion (Eq. (10)) can be related to the load expansion (Eq. (6)) through a simple integration across the bearing pad area (Eq. (3)). Δz and $\Delta \dot{z}$ are independent of x and y and do not affect the integration. As a result, the integration process can be performed separately for each order. Collecting similar order terms, the oil film coefficients through second order ($n = 2$) are

$$\begin{aligned} W_o &= I[P_o], \\ k_z &= I[P_z], \\ b_{\dot{z}} &= I[P_{\dot{z}}], \\ k_{zz} &= I[P_{zz}], \\ b_{\dot{z}\dot{z}} &= I[P_{\dot{z}\dot{z}}] = 0, \\ c_{z\dot{z}} &= I[P_{z\dot{z}}], \end{aligned} \tag{13}$$

where $I[\,] = \int_0^B \int_0^L [\,]dxdy$.

2.4 Nonlinear Stiffness and Damping Coefficients. For the purpose of representation, the classical definition of stiffness and damping coefficients is used to define a set of nonlinear stiffness and damping coefficients from the nonlinear load function (Eq. (6)). Defining the nonlinear stiffness as

$$k_{nl}(\Delta z) = \left.\frac{\partial W}{\partial(\Delta z)}\right|_{\Delta \dot{z} = \text{constant} = 0},$$

we then have

$$k_{nl}(\Delta z) = k_z + k_{zz}[\Delta z] + \tfrac{1}{2}k_{zzz}[\Delta z]^2 + \tfrac{1}{6}k_{zzzz}[\Delta z]^3 + O([\Delta z]^4). \tag{14}$$

Similarly, defining the nonlinear damping as

$$b_{nl}(\Delta z) = \left.\frac{\partial W}{\partial(\Delta \dot{z})}\right|_{\Delta z = \text{constant} \neq 0},$$

we have

$$b_{nl}(\Delta z) = b_{\dot{z}} + c_{z\dot{z}}[\Delta z] + \tfrac{1}{2}c_{zz\dot{z}}[\Delta z]^2 + \tfrac{1}{6}c_{zzz\dot{z}}[\Delta z]^3 + O([\Delta z]^4). \tag{15}$$

All the damping terms $b_{\dot{z}}, b_{\dot{z}\dot{z}}, \ldots$ except the linear term $b_{\dot{z}}$ are zero in the expansion.

The present approach allows the decoupling of the dynamic characteristics of a bearing type from the rotor system. Using this representation, the nonlinear load function will now appear as

$$W(\Delta z, \Delta \dot{z}) = W_o + k_{nl}(\Delta z)[\Delta z] + b_{nl}(\Delta z)[\Delta \dot{z}]. \tag{16}$$

2.5 Error Function. An error function is defined for the investigation of modeling error due to the truncation of higher order terms in the load expansion. Rearranging the time-dependent Reynolds' equation (Eq. (1)) and making use of Eq. (7) and Eq. (9), the error function is defined as

$$E(\Delta z, \Delta \dot{z}) = \frac{\partial}{\partial x}\left[(h_s + \Delta z)^3 \frac{\partial P}{\partial x}\right] + \frac{\partial}{\partial y}\left[(h_s + \Delta z)^3 \frac{\partial P}{\partial y}\right] - 6\mu U \frac{\partial(h_s + \Delta z)}{\partial x} - 12\mu(\Delta \dot{z}). \tag{17}$$

This function is an indicator of the degree of nonlinearity within the oil film forces. To declare a valid region for a particular order of pressure perturbation, the error function can be further normalized by the largest term within the perturbation space, i.e.,

$$E_{\text{norm}}(\Delta z, \Delta \dot{z}) = \frac{E(\Delta z, \Delta \dot{z})}{|\text{Largest Perturbation Term}|}. \tag{18}$$

Using the above definition, if the solution is perfect, $E_{\text{norm}} = 0$. The valid space for an nth order perturbation lies within a normalized error E_{norm} of [0, 1]. The degree of nonlinearity is measured as a fraction of the largest perturbation term.

2.6 Numerical Solution

2.6.1 Numerical Scheme. The relationships in Eq. (12) are in similar form. To reduce the number of variables under study, Eq. (12) is normalized. A finite difference approach is developed for the following standard normalized form of Reynolds' equation

$$\frac{\partial}{\partial \bar{x}}\left[\bar{h}^3 \frac{\partial \bar{P}_n}{\partial \bar{x}}\right] + \left(\frac{L}{B}\right)^2 \frac{\partial}{\partial \bar{x}}\left[\bar{h}^3 \frac{\partial \bar{P}_n}{\partial \bar{x}}\right] = f_n, \tag{19}$$

or

$$L[\bar{P}_n] = f_n;\ n = o, z, \dot{z}, zz, \dot{z}\dot{z}, z\dot{z}, \ldots,$$

where $\bar{h} = (h/h_o)$ is the normalized film thickness, $\bar{x} = (x/L)$ is the normalized length coordinate, $\bar{y} = (y/B)$ is the normalized breadth coordinate, f_n is the forcing function on the right-hand side of Eq. (12), and the normalization for the pressure related quantities $\bar{P}_n$ varies for different orders. $\bar{P}_n$ through second order ($n = 2$) are listed below:

Order	*Normalized pressure*	*Normalized coefficient*
$O[1]$	$\bar{P}_o = \frac{P_o h_o^2}{\mu U L}$	$\bar{W}_o = \frac{W_o h_o^2}{\mu U L^2 B}$,
$O[\Delta z]$	$\bar{P}_z = \frac{P_z h_o^3}{\mu U L}$	$\bar{k}_z = \frac{k_s h_o^3}{\mu U L^2 B}$,
$O[\Delta \dot{z}]$	$P_{\dot{z}} = \frac{P_{\dot{z}} h_o^3}{\mu L^2}$	$b_{\dot{z}} = \frac{b_{\dot{z}} h_o^3}{\mu L^3 B}$,
$O[(\Delta z)^2]$	$\bar{P}_{zz} = \frac{P_{zz} h_o^4}{\mu U L}$	$\bar{k}_{zz} = \frac{k_{zz} h_o^4}{\mu U L^2 B}$,
$O[(\Delta \dot{z})^2]$	$\bar{P}_{\dot{z}\dot{z}} = 0$	$\bar{b}_{\dot{z}\dot{z}} = 0$,
$O[\Delta z, \Delta \dot{z}]$	$\bar{P}_{z\dot{z}} = \frac{P_{z\dot{z}} h_o^4}{\mu L^2}$	$\bar{c}_{z\dot{z}} = \frac{c_{z\dot{z}} h_o^4}{\mu L^3 B}$,

(20)

Given the bearing dimensions and operating parameters, Eq. (20) can be used to obtain the normalized pressures and coefficients.

Equation (19) is an elliptical equation with four boundary conditions. Applying a five-points second order central difference scheme, it can be reduced to a set of simultaneous linear equations of the form

$$a_{i,j}(\bar{P}_n)_{i+1,j} + b_{i,j}(\bar{P}_n)_{i-1,j} + c_{i,j}(\bar{P}_n)_{i,j+1} + d_{i,j}(\bar{P}_n)_{i,j-1} + e_{i,j}(\bar{P}_n)_{i,j} = f_{i,j}, \tag{21}$$

where i, j are grid points in the direction $\bar{x}$ and $\bar{y}$, respectively, and $f_{i,j}$ is the source term of Eq. (19) at grid point (i, j). The coefficients in the above equation are functions of film thickness and grid spacing. Thus, it represents a transformation of geometric parameters into flow characteristics (Maddox, 1994).

There are several approaches for solving systems of algebraic equations where the issues of grid spacing govern the algorithm selection. Considering the potential need for a fine mesh size to resolve the bearing dimensions, a relaxation method is selected. Such methods do not have grid size limitations that may exist for rapid methods or direct matrix methods (Press et al., 1994). One of the suitable relaxation methods is successive-over-relaxation (SOR) with Chebyshev acceleration (Press et al., 1994). SOR overcorrects predicted solutions at each iteration and increases the rate of convergence. On the other hand, Chebyshev acceleration causes the error norm to decrease in each iteration, thus ensuring solution convergence. This SOR method is selected for this study. A detailed discussion of the application of this method for the steady-state Reynolds' equation solution can be found in (Press et al., 1994; Maddox, 1994).

To compute the error function, the normalized form of the error function $\bar{E}$ is used,

$$\bar{E}(\Delta\bar{x}, \Delta\bar{z}) = \frac{\partial}{\partial\bar{x}}\left[(\bar{h}_s + \Delta\bar{z})^3 \frac{\partial\bar{P}}{\partial\bar{x}}\right] + \left(\frac{L}{B}\right)^2 \frac{\partial}{\partial\bar{y}}\left[(\bar{h}_s + \Delta\bar{z})^3 \frac{\partial\bar{P}}{\partial\bar{y}}\right] - 6\frac{\partial(\bar{h}_s + \Delta\bar{z})}{\partial\bar{x}} - 12(\Delta\bar{z}), \quad (22)$$

where the bearing coordinates are normalized as before, $\bar{h}_s = (h_s/h_o)$ is the normalized initial steady state film thickness, $\Delta\bar{z} = (\Delta z/ho)$ is the normalized displacement, $\Delta\bar{z} = (\Delta z/U)(L/h_o)$ is the normalized velocity, and the normalized nonlinear pressure $\bar{P}$ is given by

$$\bar{P}(\Delta\bar{x}, \Delta\bar{z}) = \bar{P}_o + \bar{P}_x(\Delta\bar{x}) + \bar{P}_z(\Delta\bar{z}) + \tfrac{1}{2}\bar{P}_{xx}(\Delta\bar{x})^2 + \tfrac{1}{2}\bar{P}_{zz}(\Delta\bar{z})^2 + \bar{P}_{xz}(\Delta\bar{x})(\Delta\bar{z}) + O[(\Delta\bar{x})^3, (\Delta\bar{z})^3]. \quad (23)$$

The process of obtaining $\bar{E}$ is relatively simple. Once the perturbation coefficients $\bar{P}_n$ are known from solving Eq. (21) using SOR, $\bar{P}$ can be computed, and $\bar{E}$ can be evaluated within the grid space as functions of normalized displacement $\Delta\bar{x}$ and normalized velocity $\Delta\bar{z}$. Error contour data are generated for further analysis.

2.6.2 Dynamic Pressure Boundary Conditions. Four boundary conditions are required to solve the elliptical equations (Eq. (19)). These conditions stem from the ambient conditions (atmospheric pressure) at the bearing inlet, outlet, and sides

$$P(x, y = 0) = P(x, y = B) = P(x = 0, y) = P(x = L, y) = P - P_{\text{atmospheric}} = 0.$$

In normalized form,

$$\bar{P}(\bar{x}, \bar{y} = 0) = \bar{P}(\bar{x}, \bar{y} = 1) = \bar{P}(\bar{x} = 0, \bar{y}) = \bar{P}(\bar{x} = 1, \bar{y}) = 0. \quad (24)$$

Letting $P = P_o + \Delta P$, where P_o is static pressure, and ΔP is dynamic pressure, $P_o = \Delta P = 0$ at the bearing edges from Eq. (24) (Lund, 1987). The dynamic pressure boundary conditions can be recast as

$$\Delta\bar{P}(\bar{x}, \bar{y} = 0) = \Delta\bar{P}(\bar{x}, \bar{y} = 1) = \Delta\bar{P}(\bar{x} = 0, \bar{y}) = \Delta\bar{P}(\bar{x} = 1, \bar{y}) = 0. \quad (25)$$

An additional condition is required because the oil film could possibly cavitate near the trailing edge and under dynamic loading. It is observed that lubricant cavitates at close to ambient pressure because of its low saturation pressure (Hamrock, 1994). The most common approach for proper establishment of the cavitation boundary is to apply the Swift-Stieber boundary condition, also known as Reynolds' boundary condition (Jacobson and Hamrock, 1983; Hamrock, 1994). The Reynolds' boundary condition obeys flow continuity and assumes zero pressure and zero pressure gradients at the cavitation boundary. This condition is selected for the present model. In mathematical form, Reynolds' boundary condition at the cavitation boundary (x^*, y^*) is

$$P(x^*, y^*) = 0,$$

$$\frac{\partial P(x^*, y^*)}{\partial x} = 0,$$

and

$$\frac{\partial P(x^*, y^*)}{\partial y} = 0. \quad (26)$$

Assuming that the static pressure P_o at the cavitation boundary is zero (Lund, 1987), the dynamic pressure boundary conditions according to Reynolds' boundary condition must be:

$$\Delta\bar{P}(\bar{x}^*, \bar{y}^*) = 0,$$

$$\frac{\partial[\Delta\bar{P}(\bar{x}^*, \bar{y}^*)]}{\partial\bar{x}} = 0,$$

and

$$\frac{\partial[\Delta\bar{P}(\bar{x}^*, \bar{y}^*)]}{\partial\bar{y}} = 0. \quad (27)$$

These conditions are implemented in the numerical solver by setting the perturbed pressure $\bar{P}_n = 0$.

2.6.3 Solution Procedure. The overall solution procedure is depicted in Fig. 2. As soon as the equilibrium bearing profile $\bar{h}_s$ is computed as a function of inlet-to-outlet ratio (h_i/h_o), the SOR solver is used to solve for the perturbed pressures. This solution process is sequential since the higher order terms are functions of the previous lower-order terms. An over-relation parameter ω_{SOR} is needed for the SOR solver. This factor overcorrects the pressure prediction based on the following relationship

$$(\bar{P}_n)_{i,j}^{k+1} = (\bar{P}_n)_{i,j}^{k} - \omega_{\text{SOR}}\frac{r_{i,j}}{e_{i,j}} \quad (28)$$

where k is the iteration step, ω_{SOR} is the over-relaxation factor, $r_{i,j}$ is the residual error, defined in the reference (Press et al., 1994), and $e_{i,j}$ is the coefficient of $(\bar{P}_n)_{i,j}$ defined in Eq. (21). In the numerical simulation, the relaxation factor (Press et al., 1994) used is

$$\omega_{\text{SOR}} = \frac{2}{1 + \sqrt{1 - \rho_{\text{Jacobi}}^2}},$$

where

$$\rho_{\text{Jacobi}} = \frac{\cos\frac{\pi}{i_{\max}} + \left(\frac{\Delta\bar{x}}{\Delta\bar{y}}\right)^2 \cos\frac{\pi}{i_{\max}}}{1 + \left(\frac{\Delta\bar{x}}{\Delta\bar{y}}\right)^2}, \quad (29)$$

where $i_{\max}$ and $j_{\max}$ are the number of grid points in the i, j directions, respectively, $\Delta\bar{x}$, $\Delta\bar{y}$ are the step sizes in the $\bar{x}$, $\bar{y}$ directions, respectively, and ρ_{Jacobi} is the spectral radius of the Jacobi iteration. The spectral radius of the Reynolds' equation

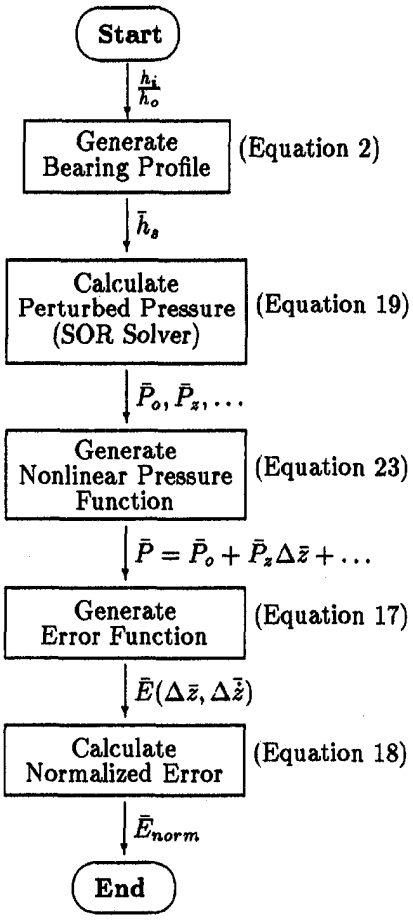

Fig. 2 Solution flow chart

is related to the rate of solution convergence. In this case, the spectral radius for Poisson's equation is used as a substitute for the unknown Reynolds' equation spectral radius (Press et al., 1994). This is valid since Reynolds' equation is of Poisson's type. The SOR solver is terminated when the final residual error norm is 10^{-5} times the initial error norm.

Once the perturbed pressures are known, the normalized nonlinear pressure $\bar{P}(\Delta\bar{x}, \Delta\bar{z})$ is generated. This function feeds directly into the evaluation of normalized error function $\bar{E}(\Delta\bar{x}, \Delta\bar{z})$. $\bar{E}$ is further normalized by the root-mean-square (RMS) value of the largest term within the perturbation space. In this case, the largest term is $(\partial/\partial\bar{x})[\bar{h}_s^3(\partial\bar{P}_{\text{perturbed}}/\partial\bar{x})]$. Contour plots of E_{norm} are generated from the error function.

3 Applications, Results, and Discussion

The linear dynamic coefficients generated from a second order nonlinear dynamic model are compared to the published results to verify the reliability of the present model. Figure 3

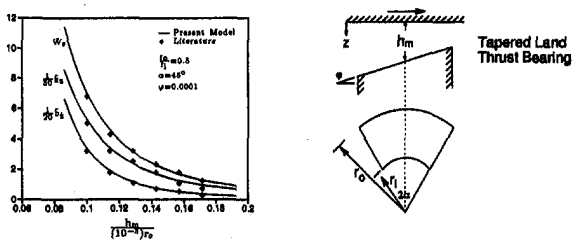

Fig. 3 Verification of the nonlinear model: a tapered land thrust bearing

shows the normalized steady-state load, linear stiffness, and linear damping coefficient of a tapered land thrust bearing at different central film thicknesses (Someya and Fukuda, 1972). Steady-state load W_s, stiffness k_z, and damping coefficient b_z in this figure are normalized as $\bar{W}_s = (W_s\epsilon^2/\mu\omega S)$, $\bar{k}_z = (k_z\epsilon^3 r_o/\mu\omega S)$, and $\bar{b}_z = (b_z\epsilon^3 r_o/\mu S)$, respectively. Here, $\epsilon = 10^{-3}$ is a constant, ω is runner angular velocity, S is sector pad area, μ is lubricant viscosity, and r_o is pad outer radius. The vertical axis in this figure represents dimensionless steady state load, stiffness, and damping coefficients, respectively. The second-order nonlinear quadratic results show good agreement with the published results in Someya and Fukuda (1972).

In the subsequent sections, the nonlinear coefficients for the conventional and MEMs slider bearing are calculated and compared to the actual curves. The accuracies of the first through fourth order nonlinear model are discussed.

3.1 1-D Nonlinear Coefficients and Higher-Order Modeling Accuracy—Conventional Slider Bearing. Using a fourth-order model, the nonlinear load function $\bar{W}$ of a conventional slider bearing with $(h_i/h_o) = 2$ and $h_o = 50$ μm is generated from the numerical solver. This load function is

$$\bar{W} = 0.069248 - 0.148477(\Delta\bar{z}) - 0.138497(\Delta\bar{z}) + \tfrac{1}{2}(0.431931)(\Delta\bar{z})^2 + 0.296953(\Delta\bar{z})(\Delta\bar{z}) - \tfrac{1}{6}(1.597596)(\Delta\bar{z})^3 - \tfrac{1}{2}(0.863861)(\Delta\bar{z})^2(\Delta\bar{z}) + \tfrac{1}{24}(7.20808249)(\Delta\bar{z})^4 + \tfrac{1}{6}(3.195191)(\Delta\bar{z})^3(\Delta\bar{z}), \quad (30)$$

and the corresponding nonlinear steady load, stiffness, and damping coefficients are

$$\bar{W}_s = 0.069248 - 0.148477(\Delta\bar{z}) + \tfrac{1}{2}(0.431931)(\Delta\bar{z})^2 - \tfrac{1}{6}(1.597596)(\Delta\bar{z})^3, + \tfrac{1}{24}(7.20808249)(\Delta\bar{z})^4 \quad (31)$$

$$\bar{k}_{nl} = 0.148477 - 0.431931(\Delta\bar{z}) + \tfrac{1}{2}(1.597596)(\Delta\bar{z})^2 - \tfrac{1}{6}(7.20808249)(\Delta\bar{z})^3, \quad (32)$$

$$\bar{b}_{nl} = 0.138497 - 0.296953(\Delta\bar{z}) + \tfrac{1}{2}(0.863861)(\Delta\bar{z})^2 - \tfrac{1}{6}(3.195191)(\Delta\bar{z})^3. \quad (33)$$

These functions can be used to obtain the dynamic characteristics of a conventional slider bearing with known displacement and velocity. Also, the accuracy of the higher order modeling results can be explored. Figure 4 shows the plot of normalized perturbation error for the first through fourth order nonlinear model as a function of static normalized displacement $\Delta\bar{z}$. Contour lines in these figures represent normalized velocity $\Delta\bar{z}$ ranges from 0 to 1. It can be seen that as displacement gets larger, the perturbation error exceeds the valid perturbation space ($\bar{E}_{\text{norm}} = 1$) rapidly. The perturbation error in some models at large displacement amplitudes can be more than 4 times the largest term in their respective perturbation spaces. This is an indication of severe nonlinearity in the oil film forces. A conventional linearized approach is therefore unacceptable. Higher order effects must be included in the hydrodynamic bearing dynamic model. Depending on the application requirement, the acceptable error criteria for a nonlinear model must be carefully selected based on the system dynamics. A 25 percent error tolerance criterion is selected for this study. This criterion allows a fourth order model to produce accurate bearing dy-

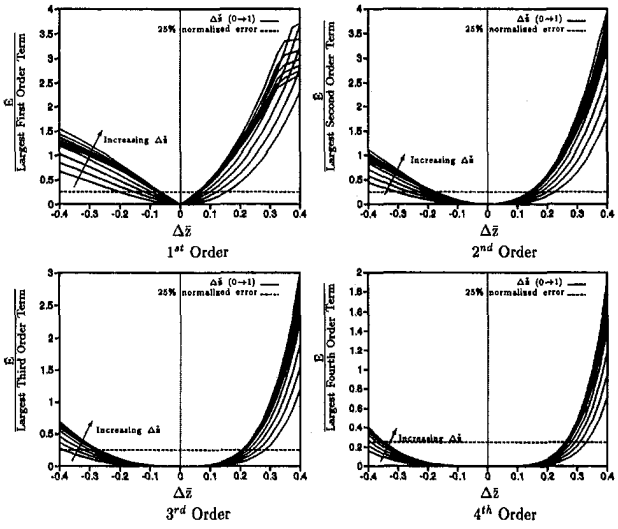

Fig. 4 Accuracy of higher order load expansion (conventional slider bearing, $h_{in}/h_{out} = 2$)

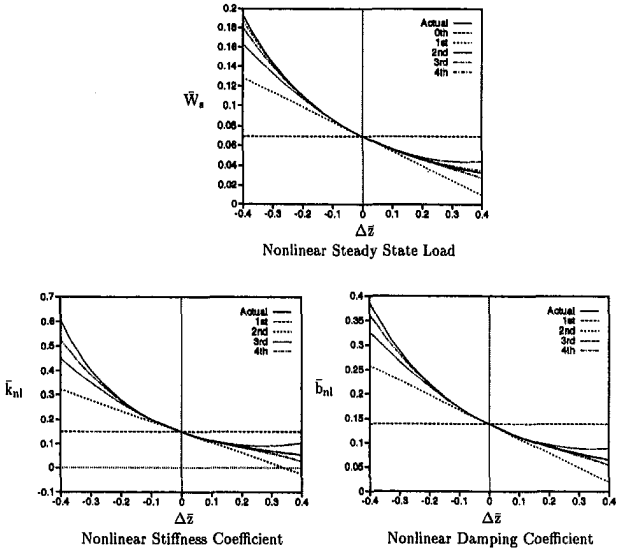

Fig. 5 Accuracy of higher order dynamic coefficients (conventional slider bearing, $h_{in}/h_{out} = 2$)

namic characteristics within a displacement amplitude of ±30 percent minimum clearance.

The valid displacement bounds for the first through fourth order model are evaluated for a 25 percent error tolerance and presented in Table 1. The ranges of validity improve as the order increases. The first order linear dynamic model is shown to be valid for a displacement of approximately ±6 percent minimum clearance. This is a much more conservative estimate than those quoted by Shapiro and Rumbarger (1971) or Lund (1987). For a fourth-order model, the designer is confident that the nonlinear dynamic results are valid within a ±30 percent minimum clearance.

The validity of the error bound and the accuracy of the higher order model are confirmed through a comparison of nonlinear steady state load, stiffness, and damping coefficients to their nonlinear curves calculated using a linear dynamic model at a small displacement increment ($\Delta\bar{z} = 0.0125$). The results are shown in Fig. 5. While the first-order results match the slope of the actual curves at the zero displacement location, the second-order results match the curvature. The subsequent orders agree closer and closer with the actual results. Significant improvement in accuracy occurs within the first few orders. Percent deviation of the higher order coefficients from their actual curves at a displacement of ±30 percent minimum clearance are evaluated and presented in Table 2. In this table, the two numbers in the bracket represent percent deviation at $(\Delta z/h_o) = -0.3$ and $(\Delta z/h_o) = 0.3$ respectively. These results show that upgrading from a first to a fourth order model improves the accuracy by more than 40%. For a fourth order model, percent deviation ranges from 1.6–7.4 at the ±30 percent minimum clearance location.

Table 2 Percent deviation of higher order coefficients from their actual curves at $\Delta z/h_o = \pm 0.3$

	% Deviation ($\Delta\bar{z} = \pm 0.3$)		
	Conventional		
Order	$\bar{W}_s$	$\bar{k}_{nl}$	$\bar{b}_{nl}$
0th	(51.6, 75.5)	—	—
1st	(20.9, 37.0)	(50.0, 48.1)	(52.2, 76.0)
2nd	(7.7, 14.3)	(25.0, 29.6)	(21.7, 36.0)
3rd	(2.7, 6.1)	(11.2, 12.9)	(7.6, 12.0)
4th	(1.6, 2.0)	(5.0, 7.4)	(2.2, 6.0)

3.2 1-D Nonlinear Coefficients and Higher Order Modeling Accuracy—MEMs Smart Slider Bearing. The nonlinear model is applied to a MEMs active smart slider bearing (Hearn et al., 1995). The MEMs smart slider bearing geometry is similar to the conventional slider bearing except that the bearing pad is populated with sensors and active actuators (Maddox, 1994). A planar view of a MEMs bearing pad is depicted in Fig. 6. Preliminary results from a MEMs smart bearing study suggest that the presence of MEMs actuators has a significant effect on the conventional bearing's steady state performance (Maddox, 1994; Masser, 1996; Wood et al., 1996). These results also suggest that a MEMs smart bearing can have controllable dynamic characteristics. This actively controllable dynamic feature can potentially be used to avoid turbomachinery instabilities such as oil whirl, critical speeds, and cavitation (Ehrich, 1992; Maddox, 1994; Masser, 1996). However, the potential effectiveness of an active MEMs bearing

Table 1 High order model lower and upper displacement bounds (25 percent normalized error)

	Displacement bounds $\left(\frac{\Delta z}{h_o}\right)$
Order	Conventional
1st	[−0.064, 0.056]
2nd	[−0.175, 0.137]
3rd	[−0.268, 0.205]
4th	[−0.344, 0.260]

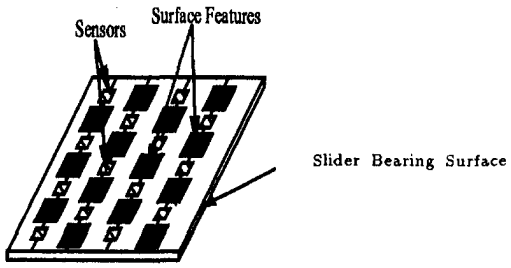

Fig. 6 Planar view of a MEMs smart bearing pad

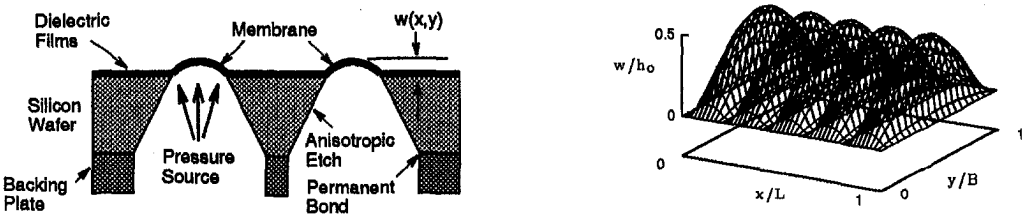

Fig. 7 Side view of a MEMs bearing pad and a MEMs membrane actuation profiler

in avoiding these instabilities depends on the magnitude of its controllable dynamic characteristics. The nonlinear model is used to determine the magnitude of the dynamic characteristic changes induced by a MEMs smart bearing.

In this analysis, the bearing pad is implanted with active membrane features without the sensors. These features are diaphragm-type actuators which can deform under an applied pressure (Maddox, 1994). A side view of the membrane feature pad is shown in Fig. 7. These features are fabricated on a silicon wafer using wafer fabrication techniques. A 2 cm by 2 cm membrane feature pad is used in this study. These membranes are activated to a height of half of the bearing minimum clearance by a pneumatic pressure source. The bearing pad profile after actuation is illustrated in Fig. 7. Bearing geometry and pad feature dimensions are summarized in Table 3.

The nonlinear load function for the application example, a MEMs slider bearing with $(h_i/h_o) = 2$ and $h_o = 50$ μm, is

$$\bar{W} = 0.107410 - 0.273233(\Delta\bar{z}) - 0.208199(\Delta\bar{z}) + \tfrac{1}{2}(0.954906)(\Delta\bar{z})^2 + 0.524181(\Delta\bar{z})(\Delta\bar{z}) - \tfrac{1}{6}(4.282986)(\Delta\bar{z})^3 - \tfrac{1}{2}(1.812075)(\Delta\bar{z})^2(\Delta\bar{z}) + \tfrac{1}{24}(23.557991)(\Delta\bar{z})^4 + \tfrac{1}{6}(8.051515)(\Delta\bar{z})^3(\Delta\bar{z}). \quad (34)$$

The resultant nonlinear steady load, stiffness, and damping functions are

$$\bar{W}_s = 0.107410 - 0.273233(\Delta\bar{z}) + \tfrac{1}{2}(0.954906)(\Delta\bar{z})^2 - \tfrac{1}{6}(4.282986)(\Delta\bar{z})^3 + \tfrac{1}{24}(23.557991)(\Delta\bar{z})^4, \quad (35)$$

Table 3 Physical dimensions of a MEMs slider bearing pad

Membrane dimension	3.5 mm (length) × 19.4 mm (width)
Inter-membrane spacing	3464 μm
Membrane-to-edge spacing	300 μm
Number of membranes	5
Minimum film thickness (h_o)	50 μm
Actuation height (w)	25 μm $\left(\frac{w}{h_o} = 0.5\right)$
Actuation direction	All Up
Inlet-to-outlet ration $\left(\frac{h_i}{h_o}\right)$	2
Length (L)	2.0 cm
Breadth (B)	2.0 cm

$$\bar{k}_{nl} = 0.273233 - 0.954906(\Delta\bar{z}) + \tfrac{1}{2}(4.282986)(\Delta\bar{z})^2 - \tfrac{1}{6}(23.557991)(\Delta\bar{z})^3, \quad (36)$$

$$\bar{b}_{nl} = 0.20819 - 0.524181(\Delta\bar{z}) + \tfrac{1}{2}(1.812075)(\Delta\bar{z})^2 - \tfrac{1}{6}(8.051515)(\Delta\bar{z})^3. \quad (37)$$

The coefficients in these nonlinear functions (Eqs. (34) – (37)) are significantly larger than those of the conventional slider bearing nonlinear functions (Eqs. (30) – (33)). Under the same dynamic conditions, then, the behavior of the MEMs slider bearing is expected to be more nonlinear than the conventional slider bearings.

3.2.1 Convergence Analysis. On a 2 cm by 2 cm baseline bearing pad, several cases are simulated to investigate the effect of mesh size on higher order dynamic coefficients. Four mesh sizes, in the order of increasing mesh density, are simulated. The calculated coefficients, together with the number of iterations required to achieve a convergence criterion of Final Residual Norm/Initial Norm $< 10^{-5}$, are calculated in Table 4. In all cases, simulations resulted in a converged solution.

Considering Table 4, a number of conclusions are apparent:

- Increasing the mesh size from 25 × 25 to 100 × 100 results in a significant change in the calculated higher-order coefficients. However, a further increase in mesh size does not increase the accuracy significantly. Thus, a 100 × 100 mesh size, corresponding to a normalized step size of $\Delta\bar{x}$: $(x/L) = \Delta\bar{y}$: $(y/B) = 0.01$, is chosen to resolve MEMS bearing features and the governing fluid mechanics of a slider bearing.
- Increasing the mesh size beyond 100 × 100 does not affect the error bound significantly. Trends are maintained across all four mesh sizes tested.
- Overall, a single uniform mesh size (100 × 100) is maintained for all simulations in this research (Figs. 4, 5, 8, and 9). This approach is a matter of choice. A uniform mesh size is desirable to extrapolate pressure data when executing the iterative solution scheme of Fig. 2. A uniform mesh of 100 × 100 may be used for this purpose, while maintaining the desired accuracy, as shown by Table 4.

3.2.2 Comparison: MEMs and Conventional Bearings. Applying the error scheme, error contour plots are generated for the MEMs nonlinear models (Fig. 8). Comparison of these plots with those of conventional slider bearing shows much higher normalized error for the MEMs slider bearing. Oil film nonlinearity is therefore more severe in a MEMs slider bearing. The valid displacement bounds for the higher order model are smaller than those of conventional slider bearing as shown in comparing Table 5 and Table 1. For a fourth-order model, the displacement bound is ±23 percent minimum clearance. More terms are required to achieve the original goal of capturing nonlinearity up to ±30 percent minimum clearance. Comparison

Table 4 Higher order coefficients for different mesh sizes

Order	25 × 25	Iterations	50 × 50	Iterations	100 × 100	Iterations	200 × 200	Iterations
$\bar{W}_o$	0.068830	98	0.069164	215	0.069248	440	0.069269	958
$\bar{k}_z$	0.147450	98	0.148270	218	0.148477	456	0.148528	965
$\bar{b}_z$	0.137660	98	0.138329	215	0.138497	440	0.138539	958
$\bar{k}_{zz}$	0.428440	109	0.431229	223	0.431931	463	0.432106	972
$\bar{c}_{z\dot{z}}$	0.294900	99	0.296541	218	0.296953	456	0.297059	965
$\bar{k}_{zzz}$	1.58235	110	1.59452	226	1.59760	469	1.59836	986
$\bar{c}_{z\dot{z}\dot{z}}$	0.856880	109	0.862458	223	0.863861	463	0.864241	972
$\bar{k}_{zzzz}$	7.12646	110	7.19174	228	7.20825	474	7.21238	1000
$\bar{c}_{zzz\dot{z}}$	3.16471	110	3.18905	226	3.19519	469	3.19673	986

of higher-order coefficients to their actual curves in Fig. 9 shows consistent trends with the error bound evaluation. In most cases, percent deviation of the higher-order coefficients from their actual values is greater for the MEMs slider bearing as shown in comparing Table 6 and Table 2. For a fourth-order model, percent deviation ranges from 1.9–15 percent at the ±30 percent minimum clearance location.

3.3 Application of Nonlinear Results: Active MEMs Smart Slider Bearing. The MEMs active smart slider bearing is realized when the membranes are actuated. Before the actuation, the MEMs slider bearing assumes the conventional slider bearing form. The actuation of all five membranes generates a significant increase in the oil film pressure. Figure 10 shows the pressure changes due to membrane actuation. This actuation manifests in an increase in nonlinear fluid film forces that can be captured by the nonlinear model. Under a constant loading condition, the bearing pad moves upward to balance the load. After the transient decays, this bearing operates with a thicker minimum gap. In this case, it is 30 percent thicker than the conventional one.

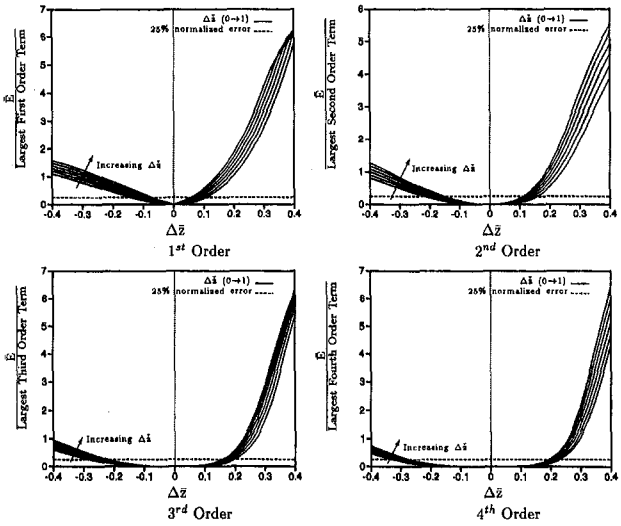

Fig. 8 Accuracy of higher order load expansion (MEMs smart slider bearings, 5 membranes, $h_{in}/h_{out} = 2$)

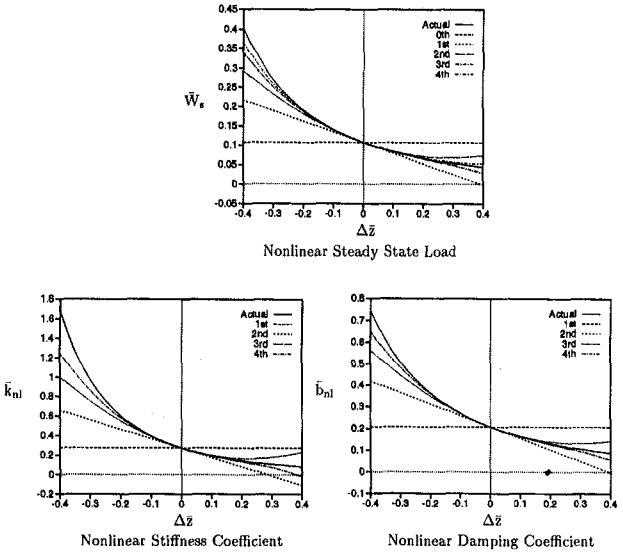

Fig. 9 Accuracy of higher order dynamic coefficients (MEMs smart slider bearing, 5 membranes, $h_{in}/h_{out} = 2$)

The nonlinear results described in the previous section are directly applicable in this active bearing. Using a fourth order nonlinear model, the maximum effects of membrane actuation are studied. Figure 11 shows the preliminary nonlinear dynamic results. Upon actuation of the active membrane, the steady state load, stiffness, and damping increase by 55, 84, and, 50 percent, respectively at the zero displacement location. Thus, the presence of membrane features alters the dynamic characteristics significantly. If the bearing displacement and velocity are known for the actuation, the time dependent load function can then be determined for this bearing.

4 Conclusion

A quasi-static nonlinear dynamic model is described in this paper. This model includes higher order terms in a typical bear-

Table 5 High order model lower and upper displacement bounds (25 percent normalized error)

	Displacement bounds $\left(\frac{\Delta z}{h_o}\right)$
Order	MEMs
1st	[−0.071, 0.056]
2nd	[−0.151, 0.112]
3rd	[−0.219, 0.157]
4th	[−0.271, 0.193]

Table 6 Percent deviation of higher order coefficients from their actual curves at $\Delta z/h_o = \pm 0.3$

	% Deviation ($\Delta\bar{z} = \pm 0.3$)		
	MEMs		
Order	$\bar{W}_s$	$\bar{k}_{nl}$	$\bar{b}_{nl}$
0th	(51.2, 48.1)	—	—
1st	(25.6, 29.6)	(60.0, 50.0)	(50.0, 48.3)
2nd	(12.2, 11.1)	(36.0, 42.5)	(24.4, 27.6)
3rd	(6.1, 7.4)	(20.0, 20.0)	(10.5, 12.1)
4th	(3.7, 1.9)	(10.7, 15.0)	(4.7, 6.9)

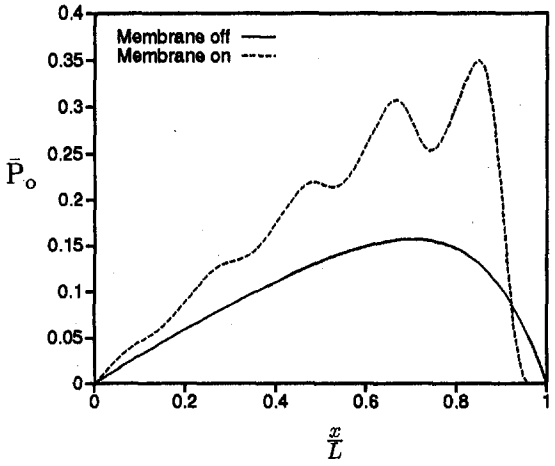

Fig. 10 Effects of membrane actuation on bearing pressure profile

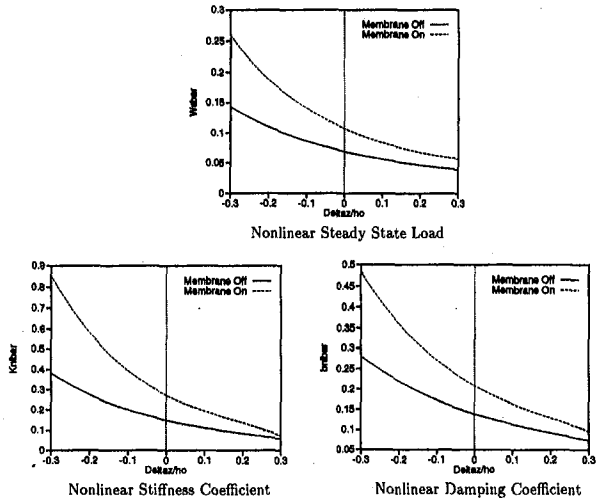

Fig. 11 Effects of membrane actuation on dynamic performance (fourth-order accuracy)

ing load expansion to capture oil film nonlinearity in the form of a nonlinear load function. It is useful in modeling bearing systems that are experiencing large dynamic motion amplitudes. An error evaluation scheme is described and used to set confidence bounds on the higher order results. Depending on the application requirements, additional terms can be added accordingly to improve the valid displacement ranges for a specific bearing application.

The new model is applied to a conventional slider bearing and a MEMs smart slider bearing. The nonlinear results suggest that oil film nonlinearity is significant, and linearized bearing coefficients are shown to be valid only within a small amplitude range (±6 percent). The nonlinear steady-state load functions, and nonlinear stiffness and damping coefficients, are evaluated for a conventional slider bearing and a MEMs smart slider bearing. These coefficients show close agreement with the actual bearing dynamic characteristics within the confidence bounds. The usefulness of present modeling approach is demonstrated through an application of the nonlinear model in an active MEMs smart slider bearing.

Acknowledgments

This study is based upon work supported, in part, by the Advanced Research Project Agency, Contract No. DABT63-92-C-0027. The authors acknowledge the input of MEMs Smart Bearing research group during the development of this modeling approach.

References

Choy, F. K., Braun, M. J., and Hu, Y., 1991, "Nonlinear Effects in a Plain Journal Bearing: Part 1—Analytical Study," ASME JOURNAL OF TRIBOLOGY, Vol. 113, pp. 555–562.

Ehrich, E. F., 1992, *Handbook of Rotordynamics,* First Ed., McGraw-Hill, New York.

Hamrock, B. J., 1994, *Fundamentals of Fluid Film Lubrication,* First Ed., McGraw-Hill, New York.

Hashi, H. E., and Sankar, T. S., 1984, "Modal Analysis and Error Estimates for Linearized Finite Journal Bearings," ASME *Journal of Vibration, Acoustics, Stress, and Reliability in Design,* Vol. 106, pp. 100–106.

Hattori, H., 1993, "Dynamic Analysis of a Rotor-Journal Bearing System with Large Dynamic Loads: Stiffness and Damping Coefficient Variations in Bearing Oil Films," *JSME International Journal,* Series C, Vol. 36(2), pp. 251–257.

Hearn, C. et al., 1995, "Smart Mechanical Bearings Using Mems Technology," *Tribology Symposium 1995,* ASME, Houston, Texas, pp. 1–10.

Jacobsen, B. O., and Hamrock, B. J., 1983, "High-Speed Motion Picture Camera Experiments of Cavitation in Dynamically Loaded Journal Bearings," ASME JOURNAL OF LUBRICATION TECHNOLOGY, Vol. 105, pp. 446–452.

Lund, J. W., 1987, "Review of the Concept of Dynamic Coefficients for Fluid Film Journal Bearings," ASME JOURNAL OF TRIBOLOGY, Vol. 109, pp. 37–41.

Maddox, W. E., 1994, "Modeling and Design of a Smart Hydrodynamic Bearing With an Actively Deformable Surface," Master's thesis, The University of Texas at Austin, Dept. of Mechanical Engineering, Austin, TX.

Masser, D. E., 1996, "An Experimental Investigation of Hydrodynamic Bearings with Micromachined Surfaces," Master's thesis, The University of Texas at Austin, Dept. of Mechanical Engineering, Austin, TX.

Pinkus, O. and Sternlicht, B., 1961, *Theory of Hydrodynamic Lubrication,* First Ed., McGraw-Hill, New York.

Press, W. H., Teukolsky, S. A., Vetterling, W. T., and Flannery, B. P., 1994, *Numerical Recipes in C. The Art of Scientific Computing,* Second Ed., Cambridge University Press, Cambridge.

Rylander, H. G., Carlson, M. J., and Lin, C. R., 1995, "Actively Controlled Bearing Surface Profiles: Theory and Experiment," *Tribology Symposium 1995,* ASME, Houston, TX, pp. 11–14.

Shapiro, W., and Rumbarger, J. H., 1971, "Bearing Influence and Representation in Rotor Dynamics Analysis," *Flexible Rotor-Bearing System Dynamics,* The Design Engineering Division, ASME, p. 2.

Someya, T., 1989, *Journal-Bearing Databook,* First Ed., Springer-Verlag, Berlin, Heidelberg.

Someya, T., and Fukuda, T., 1972, "Analysis and Experimental Verification of Dynamic Characteristics of Oil Film Thrust Bearings," *Bulletin of JSME,* Vol. 15(86), pp. 1004–1015.

Wood, K. L. et al., 1996, "Mems Hydrodynamic Bearings: Applications and Implications to Machine-Failure Prevention," Technology Showcase: Integrated Monitoring, Diagnostics, and Failure Prevention, Society of Machinery Failure Prevention Technology (MFPT), Mobile, AL, pp. 363–372.